JOM, Vol. 72, No. 6, 2020
https://doi.org/10.1007/s11837-019-03919-5

In Situ Electron Diffraction Investigation of Solid State Synthesis of Co-In_2O_3 Ferromagnetic Nanocomposite Thin Films

LIUDMILA E. BYKOVA,[1,3] SERGEY M. ZHARKOV,[1,2] VICTOR G. MYAGKOV,[1] VICTOR S. ZHIGALOV,[1] and GENNADY S. PATRIN[1,2]

1.—Kirensky Institute of Physics, Federal Research Center KSC SB RAS, Akademgorodok 50/38, Krasnoyarsk, Russia 660036. 2.—Siberian Federal University, 79 Svobodny pr., Krasnoyarsk, Russia 660041. 3.—e-mail: lebyk@iph.krasn.ru

In situ electron diffraction was used to study structural transformations during the formation of Co-In_2O_3 ferromagnetic nanocomposite thin films in a thermite reaction of In/Co_3O_4 bilayer thin films. Heating was performed from room temperature to 600°C at a rate of 4°C/min, while simultaneously electron diffraction patterns were recorded at a speed of 4 frames/min. This made it possible to determine the initiation, 185°C, and finishing, 550°C, temperatures of the solid-state synthesis, as well as the change in the phase composition during the thermite reaction. The synthesized Co-In_2O_3 film nanocomposite contained ferromagnetic cobalt nanoclusters surrounded by an In_2O_3 layer, with an average size of 20 nm, and had a magnetization of 400 emu/cm^3 and a coercivity of 50 Oe at room temperature. The estimate of the effective interdiffusion coefficient of the reaction suggests that the main mechanism for the formation of the Co-In_2O_3 nanocomposite is diffusion along the grain boundaries and dislocations.

INTRODUCTION

Composite ferromagnetic films containing nanoclusters of 3d-metals Co, Fe, and Ni in a dielectric or semiconductor matrix obtained by various physical and chemical methods, including the sol–gel method, spray pyrolysis, the microemulsion method, magnetron sputtering, pulsed laser deposition, ion implantation, and joint deposition have been intensively studied.[1–9] Although the synthesis of these nanocomposites often passes under equilibrium conditions, the magnetic and other physicochemical properties strongly depend on the fabrication technique used, the particle size and concentration, and the type of chemical bond between the nanoparticles and the matrix. Recently, there has been a surge in nonequilibrium processing of ferromagnetic composites using methods like pulsed laser irradiation,[10] pulsed laser deposition,[11] ion implantation,[12,13] and ball-milling.[14] Thermite synthesis of materials also takes place under nonequilibrium conditions. Thermites comprising of nanosized fuels, such as Al, Mg, Ti, and Zr, and oxidizers, such as SnO2, CuO, Bi2O3, NiO, Co_3O_4, and Fe2O3, are termed nanostructured metastable intermolecular composites, nanothermites or superthermites, and have been widely investigated as a subclass of nano-energetic materials. In contrast to traditional energetic materials, nanomaterials have fuel and oxidizer particles decreased to nanoscale dimensions, and possess high interfacial contact areas, which decrease the diffusion distances between the reactants. As a result, the nano-energetic materials have lower ignition temperatures, low ignition delay, an enhanced rate of energy release, extremely high heating rates, and a significant increase in the combustion velocity to several km/s.[15–18] The temperature of the combustion wave reaches several thousand degrees, which can lead to a very supercooled state and rapid quenching of the reaction product. Nanocomposites obtained under nonequilibrium conditions often have metastable phases and possess unusual magnetic and physicochemical properties.

In recent years, multilayer reactive nanotermites, consisting of alternating nanosized layers of metal fuel and oxidizing agents with a total thickness in the range from 0.1 to several microns, have

(Published online November 20, 2019)

attracted considerable attention, both for understanding reaction mechanisms and for practical applications.[19–21] Recently, a simple and effective method of solid-state synthesis of magnetic nanogranular thin films has been proposed, based on initiating thermite reactions between 3d-metal oxide films (Fe_2O_3, Co_3O_4) and In, Zr, Zn, and Al metals, whose oxides are wide-gap semiconductors or dielectrics.[22–28] Such an approach makes it possible to obtain thin single-layer and multilayer nanogranular films with a well-controlled size and distribution of magnetic granules over the thickness of the film.[26] Among several types of nano-energetic materials, multilayer nanofilms are a simple model system, both for the theoretical and experimental study of atomic transfer across the interface. However, the fundamental reaction mechanisms at the nanoscale remain unclear. Important steps in this direction can be provided by the studies of scenarios of the initial reaction stage on the interface between the two reactive nanolayers.

This paper presents the results of investigations of the structural properties of the Co-In_2O_3 nanocomposite thin films obtained by initiating a thermite reaction in a In/Co_3O_4 bilayer film system. Indium oxide (In_2O_3) is a wide-gap *n*-type semiconductor characterized by a high concentration of free electrons in combination with transparency in the visible range of electromagnetic radiation.[29] This provides a variety of practical applications of this oxide. Co-In_2O_3 nanocomposites and cobalt-doped In_2O_3 attract attention due to their possible use in optoelectronic and spintronic devices and gas sensors.[30–36]

The study of the formation processes of Co-In_2O_3 nanocomposite thin films was carried out directly in the column of a transmission electron microscope (TEM) by heating the film sample of In/Co_3O_4 from room temperature to 600°C. In situ electron diffraction was used to study the structural transformations during the solid-state reaction. This method had previously been successfully used by the authors to study solid-state reactions in thin-film systems: Fe/Pd,[37,38] Cu/Au,[39] Fe/Si,[40] Al/Pt.[41] In this paper, in situ electron diffraction for thermite reactions in thin films was used for the first time. The initiation and finishing temperatures of the thermite reaction, which occurred between the In and Co_3O_4 nanolayers and the phase composition of the reaction products, were determined. An estimate of the effective interdiffusion coefficient of the reaction was given.

EXPERIMENTAL PROCEDURES

Figure 1 illustrates the process of the fabrication of the Co-In_2O_3 nanocomposite thin films. The thicknesses of the Co and In layers in the In/Co_3O_4 bilayer films were chosen according to the equation of thermite reaction (1):

$$3Co_3O_4 + 8In = 4In_2O_3 + 9Co \qquad (1)$$

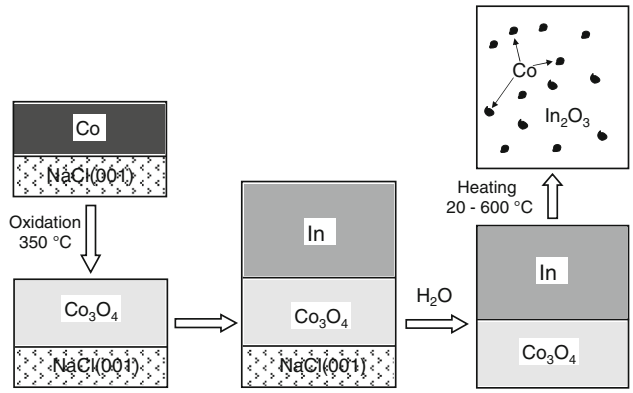

Fig. 1. Illustration of the solid-state synthesis of the Co-In_2O_3 nanocomposite thin films.

For a solid-state reaction to occur, the reagents must satisfy the condition that their formation enthalpy (ΔH) must be higher than the formation enthalpy of the reaction products. For reaction (1), this condition is satisfied: $\Delta H(Co_3O_4) = -891$ kJ/mol is higher than $\Delta H(In_2O_3) = -925.8$ kJ/mol.[42]

The fabrication of the initial bilayer In/Co_3O_4 films was carried out in several stages:

1. Thermal deposition of Co films with a thickness of $\sim$ 20 nm in a vacuum at a residual pressure of 1.3×10^{-7} kPa on the fresh cleaved single crystal of the NaCl(001) substrate;
2. Formation of Co_3O_4 films by air oxidation of the Co layers at 350°C for 30 min.;
3. Thermal deposition of the In layer with a thickness of $\sim$ 35 nm in a vacuum at a residual pressure of 1.3×10^{-7} kPa onto the Co_3O_4 film surface. To prevent an uncontrolled reaction between the In and Co_3O_4 layers, In was deposited on the substrate at room temperature. Materials of a high level of purity were used for the evaporation: Co (99.98%), and In (99.995%).[43] The In and Co layer thicknesses were determined by x-ray fluorescence analysis. The total thicknesses of the bilayer films under study were 55–60 nm.
4. The In/Co_3O_4/NaCl(001) films were separated from the NaCl(001) substrate in bidistilled water at room temperature.

The structure and local elemental composition of the samples were studied using a JEOL JEM-2100 TEM equipped with an Oxford Inca x-sight energy dispersive spectrometer at an accelerating voltage of 200 kV, and a special sample holder (Gatan heating holder, model 652 with a double tilt), which allows for monitoring the sample during heating from room temperature to temperatures up to 1000°C.

As part of this work, the authors carried out in situ electron diffraction investigations of the processes of the thermite synthesis of Co-In_2O_3 nanocomposite films by thermal heating in In/Co_3O_4

bilayer films. For this purpose, In/Co_3O_4 bilayer films placed on a molybdenum TEM grid were heated from room temperature to 600°C at a rate of 4°C/min. Simultaneously with the heating, electron diffraction patterns were registered (at a speed of 4 frames/min) and synchronous sample temperature measurements were carried out. This made it possible to obtain information on the initiation and finishing temperatures of the thermite reaction, and on the change in the phase sequence during the process of synthesis between the In and Co_3O_4 nanolayers. The analysis of the intensity of the electron diffraction reflections and the interpretation of the electron diffraction patterns were made using the Gatan Digital Micrograph software and the ICDD PDF 4+ crystallographic database.[44]

The saturation magnetization was measured on an MPMS-XL SQUID magnetometer (Quantum Design) on in-plane magnetic fields.

RESULTS AND DISCUSSION

The initial In/Co_3O_4 samples were bilayer thin films consisting of In and Co_3O_4 nanolayers. The electron diffraction pattern (Fig. 2a), obtained from the initial In/Co_3O_4 film by the method of selected area electron diffraction from an area with a diameter of ~ 1 μm, has complete sets of diffraction reflections of a polycrystalline type, characteristic of the phases: In (the space group 4/mmm, lattice constants: a = 3.252 Å, c = 4.9466 Å, PDF Card # 04-004-7737) and Co_3O_4 (the space group Fd-3m, lattice constant a = 8.0837 Å, PDF Card # 00-042-1467).

The sample was heated from room temperature to 600°C at a rate of 4°C/min in the TEM column (in situ electron diffraction mode). When the temperature was near the melting point of indium, 157°C, the reflections of In disappeared from the electron diffraction pattern (Fig. 2b) and only the reflections from Co_3O_4 remained. The diffraction pattern did not change until the temperature reached 185°C (Fig. 3), when, in addition to the reflections corresponding to the Co_3O_4 phase, diffraction reflections appeared corresponding to interatomic distances (111) and (200) fcc-Co (the space group Fm-3m, lattice constant a = 3.5447 Å, PDF Card # 00-015-0806) and diffraction reflections corresponding to the In_2O_3 phase (the space group Ia-3, lattice constant a = 10.118 Å, PDF Card # 00-006-0416). The appearance of the diffraction reflections corresponding to the fcc-Co and In_2O_3 phases indicates the beginning of thermite reaction (1) of the reduction of Co from Co_3O_4 to form In_2O_3.

During the heating process, when the sample temperature reached 400°C, a sharp change in the set of the diffraction reflections in the electron diffraction pattern was observed (see Fig. 4a). The reflections from the Co_3O_4 phase disappear and reflections from the hcp-Co phase appear (the space group $P6_3/mmc$, lattice constants a = 2.5071 Å, c = 4.08686 Å, PDF Card # 04-001-3273) and reflections from the CoO phase (the space group Fm-3 m, lattice constant a = 4.2612 Å, PDF Card # 00-048-1719) are also present in the film in a small quantity.

When the sample was heated to 550°C, the intensity of the diffraction reflections increased, which is related to the reaction relaxation processes,

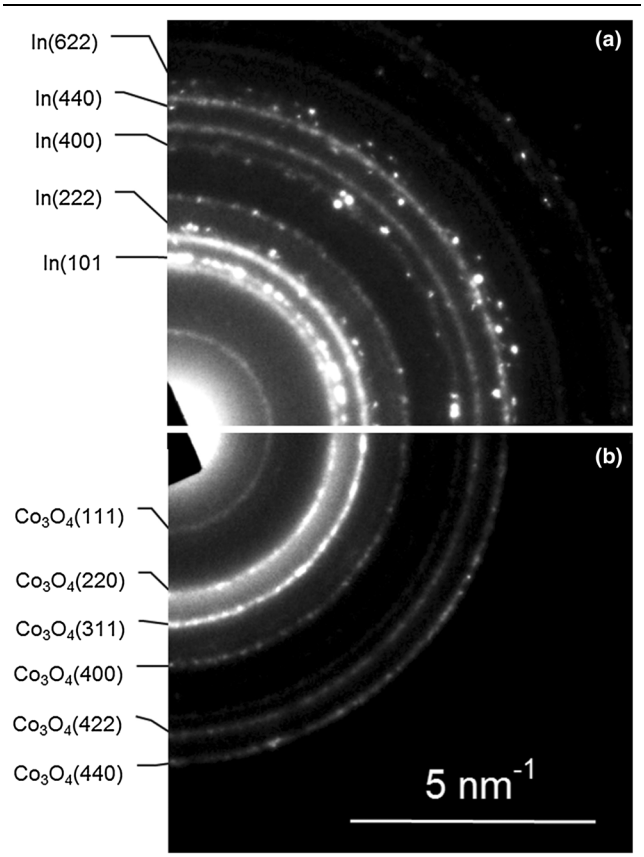

Fig. 2. Electron diffraction patterns obtained from the In/Co_3O_4 film in the initial state (a) and at a temperature of 157°C (b).

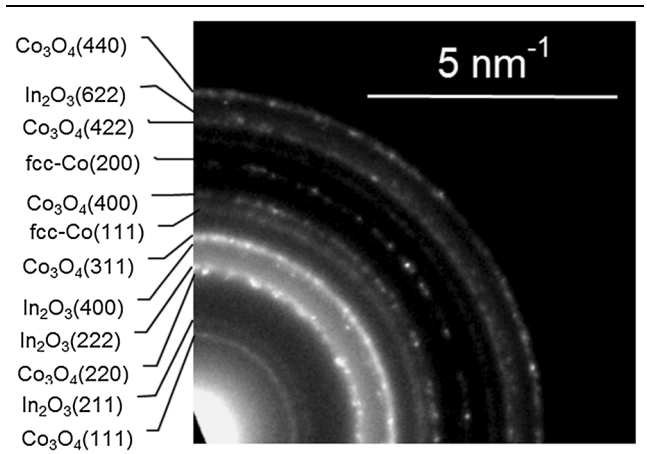

Fig. 3. Electron diffraction pattern obtained from the In/Co_3O_4 film at a temperature of 185°C.

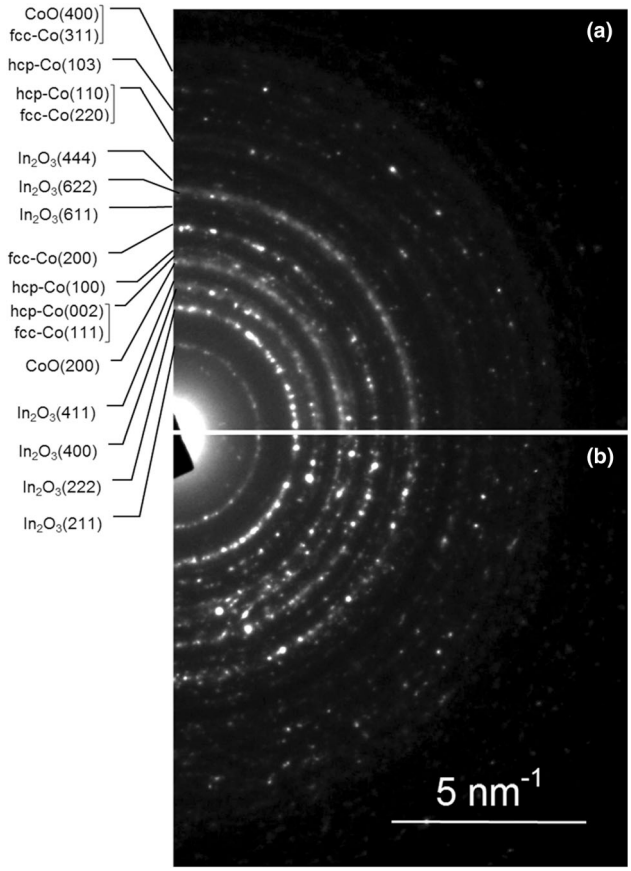

Fig. 4. Electron diffraction patterns obtained from the In/Co_3O_4 film at temperatures of 400°C (a) and 600°C (b).

including the increase of the size of the Co grains and the improvement of the crystal quality in the insulating In_2O_3 matrix, but no new phases were formed. Further heating to 600°C did not lead to a change in the set of diffraction reflections in the electron diffraction pattern (see Fig. 4b). The cooling of the sample to room temperature also did not lead to a change in the intensity and set of diffraction reflections in the electron diffraction pattern. According to the electron diffraction data, the reaction was completely finished at a temperature of ~ 550°C.

The TEM (Fig. 5), scanning TEM (Fig. 6a) and energy dispersive spectroscopy (EDS) elemental mapping images of Co, In and O (Fig. 6b, c, and d), obtained from the In/Co_3O_4 film after heating the sample to 600°C, show that the Co nanoparticles are uniformly distributed in the reaction product. From the histogram (inset in Fig. 5), it follows that the average diameter of the Co nanoparticles is ~ 20 nm. However, Co nanoparticles smaller than 4 nm were not included in the histogram, since they are not visible in the TEM image. These data confirm that, during the heating of the In/Co_3O_4 film, cobalt was reduced from the cobalt oxide as a result of the thermite reaction (1), and the Co-In_2O_3 nanocomposite was formed.

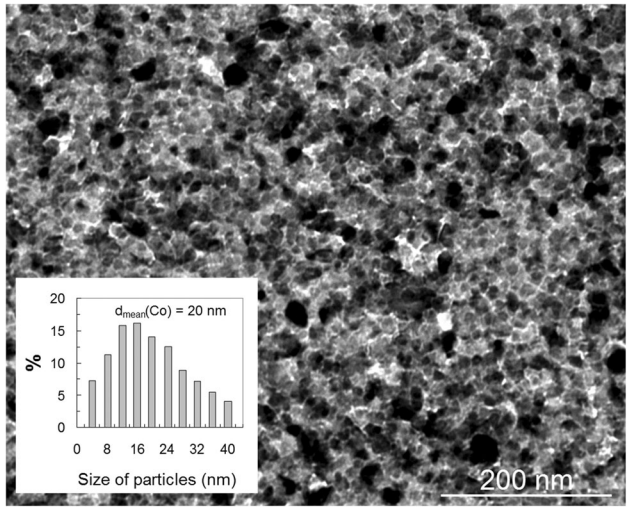

Fig. 5. TEM image of the In/Co_3O_4 film after heating to 600°C. Inset histogram of the size distribution of the Co nanoparticles.

From the results of the study, it follows that the initiation temperature, T_{in}, of the thermite reaction (1) in the In/Co_3O_4 thin-film system is 185°C, and the finishing temperature, T_{fin}, of reaction (1) is 550°C. During the heating of the In/Co_3O_4 film system, a sequence of phases was observed:

$$Co_3O_4 + In \xrightarrow{185^\circ C} Co_3O_4 + In_2O_3 + fccCo \xrightarrow{400^\circ C} hcpCo + fccCo + In_2O_3 + CoO \quad (2)$$

From the foregoing, it follows that the reaction (1) starts at a temperature of initiation $T_{in} \sim 185$°C and, at a temperature of 400°C, the reaction occurs at a diffusion length equal to the total film thickness, d = 55 nm. At a rate of 4°C/min, the heating from 185°C to 400°C corresponds to a reaction time $t \sim 3.3 \times 10^3$ s. Assuming a weak temperature dependence of diffusion in the 185–400°C temperature range, and using the equation for reaction–diffusion, $d^2 = 6D_{eff}\,t$, we can estimate the order of the effective diffusion coefficient, $D_{eff} \sim 0.9 \times 10$ 14 cm^2/s. It has been experimentally established that diffusion along surfaces, dislocations, and grain boundaries (GBs) is several orders of magnitude faster than bulk diffusion.[45] Fast GB diffusion plays a predominant role in the atomic migration in solids and solid-state thin-film synthesis. The experimental values of GB diffusion coefficients in thin films for most metals have (10^{-12}–10^{-18}) cm^2/s values in the 100–800°C temperature range.[46–50] It can be assumed that this mechanism is the main process that controls the atomic transfer through the layers of the reaction product.

Thermite mixtures react with a release of large quantities of heat and may have a self-propagating high-temperature synthesis mode. For the most reactive bilayers connected to the substrate, the solid-state reaction between the layers starts in a self-propagating mode only above the initiation

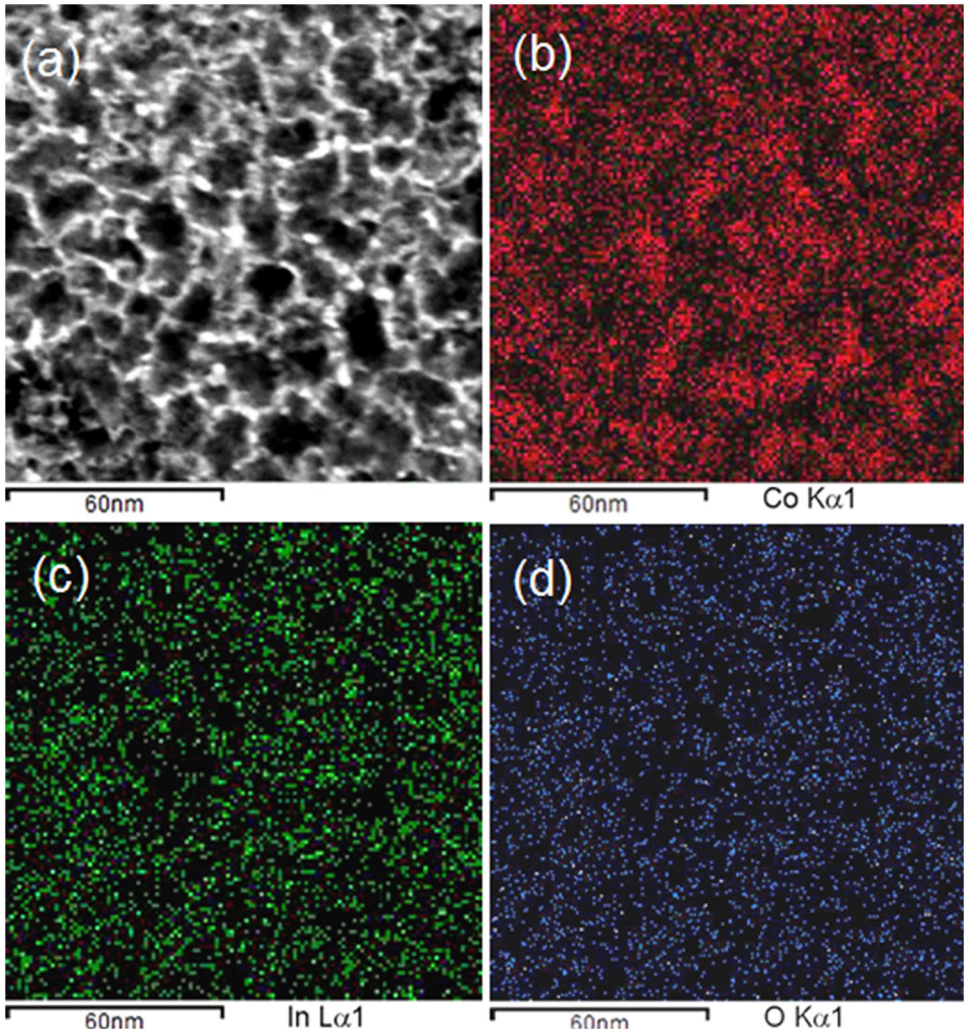

Fig. 6. Scanning TEM image (a) of the In/Co_3O_4 film after heating to 600°C and the corresponding EDS elemental mapping images of Co (b), In (c) and O (d).

temperature, T_{in}, and with a heating rate exceeding > 20 K/s.[22] In our case, at heating rates < 20 K/s, the reaction proceeds in the reaction–diffusion mode.

Figure 7 shows the room-temperature hysteresis loop for the synthesized Co-In_2O_3 nanocomposite thin film, according to which the film magnetization is 400 emu/cm^3 and the coercivity is about 50 Oe. These values are stable and do not change with time. The absence of saturation in fields stronger than the coercivity suggests that the synthesized Co-In_2O_3 samples contain a certain amount of superparamagnetic Co nanoparticles (d < 20 nm).[51] These particles, and disordered spins at the Co/In_2O_3 interface, contribute to the strong-field portion of the hysteresis loop of the Co-In_2O_3 thin film. The relatively large ratio, $M_r/M_s \sim 0.5$, between the remanent magnetization M_r and the saturation magnetization M_s (Fig. 7), shows that the Co nanoparticles consist of randomly oriented grains with a cubic magnetocrystalline anisotropy.[52]

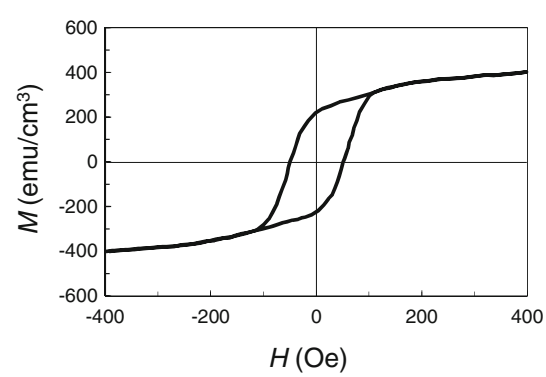

Fig. 7. In-plane hysteresis loop of the synthesized Co-In_2O_3 nanocomposite thin film at room temperature.

CONCLUSION

The main results of our investigations are as follows. The synthesis of ferromagnetic Co-In_2O_3 thin-film nanocomposites in the In/Co_3O_4 layered system was obtained using a thermite reaction:

$3Co_3O_4 + 8In = 4In_2O_3 + 9Co$. In situ electron diffraction was used to study the structural transformations during the thermite reaction. The heating was performed directly in the transmission electron microscope column by heating the film sample of In/Co_3O_4 from room temperature to 600°C at a rate of 4°C/min, with the simultaneous registration of the electron diffraction patterns. A complex of structural and magnetic investigations unambiguously revealed the formation of ferromagnetic cobalt nanoclusters with an average size of 20 nm embedded in the In_2O_3 matrix. The synthesized $Co\text{-}In_2O_3$ film nanocomposites had a magnetization of about 400 emu/cm^3 and a room-temperature coercivity of about 50 Oe. The initiation, 185°C, and finishing, 550°C, temperatures of synthesis and the phase composition of the reaction products were determined. The effective interdiffusion coefficient, $D_{\text{eff}} \approx 0.9 \times 10^{-14}$ cm^2/s, was estimated, and corresponded to the diffusion coefficient along the grain boundaries and dislocations. Thus, the thermite method is promising for synthesizing ferromagnetic nanocomposite thin films consisting of ferromagnetic nanoparticles.

ACKNOWLEDGEMENTS

The investigation was conducted under the partial financial support of the Russian Foundation for Basic Research (Grants #18-03-01173 and #19-43-240003).

CONFLICT OF INTEREST

The authors declare that they have no conflict of interest.

REFERENCES

1. C.-W. Nan and J. Quanxi, *MRS Bull.* 40, 719 (2015). https://doi.org/10.1557/mrs.2015.196.
2. S. Behrens, *Nanoscale* 3, 877 (2011). https://doi.org/10.1039/C0NR00634C.
3. X. Batlle and A. Labarta, *J. Phys. D* 35, R15 (2002). https://doi.org/10.1088/0022-3727/35/6/201.
4. A.K. Rathore, S.P. Pati, M. Ghosh, A. Roychowdhury, and D. Das, *J. Mater. Sci. Mater. Electron.* 28, 6950 (2017). https://doi.org/10.1007/s10854-017-6395-7.
5. G.-R. Xu, J.-J. Shi, W.-H. Dong, Y. Wen, X.-P. Min, A.-P. Tang, J. Xu, H. Yang, W. Fu, W. Fan, Q. Zhu, and G. Zou, *J. Alloys Compds.* 630, 266 (2015). https://doi.org/10.1016/j.jallcom.2015.01.067.
6. E.B. Dokukin, R.V. Erhan, A.Kh. Islamov, M.E. Dokukin, N.S. Perov, and E.A. Gan'shina, *Phys. Status Solidi B* 250, 1656 (2013). https://doi.org/10.1002/pssb.201248379.
7. R. Goyal, S. Lamba, and S. Annapoorni, *Phys. Status Solidi A* 213, 1309 (2016). https://doi.org/10.1002/pssa.201532704.
8. B. Gokul, P. Saravanan, V.T.P. Vinod, M. Černík, and R. Sathyamoorthy, *Powder Technol.* 274, 98 (2015). https://doi.org/10.1016/j.powtec.2015.01.002.
9. Y. Cao, N. Kobayashi, Y.-W. Zhang, S. Ohnuma, and H. Masumoto, *J. Appl. Phys.* 122, 133903-1 (2017). https://doi.org/10.1063/1.5005620.
10. S. Gupta, R. Sachan, A. Bhaumik, and J. Narayan, *Nanotechnology* 29, 1 (2018). https://doi.org/10.1088/1361-6528/aadd75.
11. Q. Dai, D. Wu, K. Guo, J. Zhang, M. Zhang, R. Cui, and C. Deng, *J. Mater. Sci. Mater. Electron.* 29, 17333 (2018). https://doi.org/10.1007/s10854-018-9828-z.
12. S. Zhou, K. Potzger, J. von Borany, R. Grotzschel, W. Skorupa, M. Helm, and J. Fassbender, *Phys. Rev. B* 77, 035209-1 (2008). https://doi.org/10.1103/PhysRevB.77.035209.
13. P. Satyarthi, S. Ghosh, P. Mishra, B.R. Sekhar, F. Singh, P. Kumar, D. Kanjilal, R.S. Dhaka, and P. Srivastava, *J. Magn. Magn. Mater.* 385, 318 (2015). https://doi.org/10.1016/j.jmmm.2015.03.029.
14. N.R. Panda, S.P. Pati, A. Das, and D. Das, *Appl. Surf. Sci.* 449, 654 (2017). https://doi.org/10.1016/j.apsusc.2017.12.003.
15. E.L. Drezin, *Prog. Energy Combust. Sci.* 35, 141 (2009). https://doi.org/10.1016/jpecs.2008.09.001.
16. Y. Yang, D.-R. Yan, Y.-C. Dong, X.-G. Chen, L. Wang, Z.-H. Chu, J.-X. Zhang, and J.-N. He, *J. Alloys Compd.* 579, 1 (2013). https://doi.org/10.1016/j.jallcom.2013.05.045.
17. A.S. Mukasyan and A.S. Rogachev, *Adv. Power Technol.* 26, 654 (2015). https://doi.org/10.1016/j.apt.2015.03.013.
18. X. Zhou, M. Torabi, J. Lu, R. Shen, and K. Zhang, *ACS Appl. Mater. Interfaces* 6, 3058 (2014). https://doi.org/10.1021/am4058138.
19. A.H. Kinsey, K. Slusarski, S. Sosa, and T.P. Weihs, *ACS Appl. Mater. Interfaces* 9, 22026 (2017). https://doi.org/10.1021/acsami.7b03071.
20. I. Abdallah, J. Zapata, G. Lahiner, B. Warot-Fonrose, J. Cure, Y. Chabal, A. Esteve, and C. Rossi, *ACS Appl. Energy Mater.* 1, 1762 (2018). https://doi.org/10.1021/acsaem.8b00296.
21. J. Zapata, A. Nicollet, B. Julien, G. Lahiner, A. Esteve, and C. Rossi, *Combus. Flame* 205, 389 (2019). https://doi.org/10.1016/j.combustflame.2019.04.031.
22. V.G. Myagkov, I.A. Tambasov, O.A. Bayukov, V.S. Zhigalov, L.E. Bykova, Y.L. Mikhlin, M.N. Volochaev, and G.N. Bondarenko, *J. Alloys Compds.* 612, 189 (2014). https://doi.org/10.1016/j.jallcom.2014.05.176.
23. I.A. Tambasov, K.O. Gornakov, V.G. Myagkov, L.E. Bykova, V.S. Zhigalov, A.A. Matsynin, and E.V. Yozhikova, *Phys. B* 478, 135 (2015). https://doi.org/10.1016/j.physb.2015.08.054.
24. L.E. Bykova, V.S. Zhigalov, V.G. Myagkov, M.N. Volochaev, A.A. Matsynin, G.N. Bondarenko, and G.S. Patrin, *Phys. Solid State* 60, 2072 (2018). https://doi.org/10.1134/S1063783418100049.
25. V.G. Myagkov, L.E. Bykova, V.S. Zhigalov, A.A. Matsynin, M.N. Volochaev, I.A. Tambasov, YuL Mikhlin, and G.N. Bondarenko, *J. Alloys Compds.* 724, 820 (2017). https://doi.org/10.1016/j.jallcom.2017.07.081.
26. M.N. Volochaev, S.V. Komogortsev, V.G. Myagkov, L.E. Bykova, V.S. Zhigalov, N.P. Shestakov, D.A. Velikanov, D.A. Smolyakov, A.V. Lukyanenko, V.B. Rachek, Y.Y. Loginov, I.A. Tambasov, and A.A. Matsynin, *Phys. Solid State* 60, 1425 (2018). https://doi.org/10.1134/s1063783418070302.
27. V.G. Myagkov, L.E. Bykova, O.A. Bayukov, V.S. Zhigalov, I.A. Tambasov, S.M. Zharkov, A.A. Matsynin, and G.N. Bondarenko, *J. Alloys Compds.* 636, 223 (2015). https://doi.org/10.1016/j.jallcom.2015.02.012.
28. V.G. Myagkov, V.S. Zhigalov, L.E. Bykova, S.M. Zharkov, A.A. Matsynin, M.N. Volochaev, I.A. Tambasov, and G.N. Bondarenko, *J. Alloys Compds.* 665, 197 (2016). https://doi.org/10.1016/j.jallcom.2015.12.257.
29. C.H. Liang, G.W. Meng, Y. Lei, F. Phillipp, and L.D. Zhang, *Adv. Mater.* 13, 1330 (2001). https://doi.org/10.1002/1521-4095(200109)13:17%3c1330::AID-ADMA1330%3e3.0.CO;2-6.
30. Z.-K. Tang, L.-M. Tang, D. Wang, L.-L. Wang, and K.-Q. Chen, *EPL* 97, 57006-1 (2012). https://doi.org/10.1209/0295-5075/97/57006.

31. X. Meng, L. Tang, and J. Li, *J. Phys. Chem. C* 114, 17569 (2010). https://doi.org/10.1021/jp106767n.
32. R. Mukherji, V. Mathur, A. Samariya, and M. Mukherji, *JAN* 2, 105 (2017). https://doi.org/10.22606/jan.2017.22003.
33. N.H. Hong, J. Sakai, N.T. Huong, and V. Brizé, *J. Magn. Magn. Mater.* 302, 228 (2006). https://doi.org/10.1016/j.jmmm.2005.09.010.
34. M.Z. Naik and A.V. Salker, *Mater. Res. Innov.* 21, 237 (2017). https://doi.org/10.1080/14328917.2016.1207044.
35. Z. Li and Y. Dzenis, *Talanta* 85, 82 (2011). https://doi.org/10.1016/j.talanta.2011.03.033.
36. Z. Wang, C. Hou, Q. De, F. Gu, and D. Han, *ACS Sens.* 3, 468 (2018). https://doi.org/10.1021/acssensors.7b00896.
37. S.M. Zharkov, E.T. Moiseenko, R.R. Altunin, N.S. Nikolaeva, V.S. Zhigalov, and V.G. Myagkov, *JETP Lett.* 99, 405 (2014). https://doi.org/10.1134/S0021364014070145.
38. E.T. Moiseenko, R.R. Altunin, and S.M. Zharkov, *Phys. Solid State* 59, 1233 (2017). https://doi.org/10.1134/S1063783417060154.
39. S.M. Zharkov, E.T. Moiseenko, and R.R. Altunin, *J. Solid State Chem.* 269, 36 (2019). https://doi.org/10.1016/j.jssc.2018.09.009.
40. R.R. Altunin, E.T. Moiseenko, and S.M. Zharkov, *Phys. Solid State* 60, 1413 (2018). https://doi.org/10.1134/S106378341807003X.
41. S.M. Zharkov, R.R. Altunin, E.T. Moiseenko, G.M. Zeer, S.N. Varnakov, and S.G. Ovchinnikov, *Solid State Phenom.* 215, 144 (2014). https://doi.org/10.4028/www.scientific.net/SSP.215.144.
42. W.M. Haynes, eds., *CRC Handbook of Chemistry and Physics*, 97th ed. (Boca Raton: CRC Press, 2016), p. 2670.
43. ADVENT Research Materials Ltd., Oxford, U.K. www.advent-rm.com.
44. Powder Diffraction File (PDF 4+, 2018), Inorganic Phases Database, International Center for Diffraction Data (ICDD), Swarthmore, PA, USA. http://www.icdd.com/products/pdf4.htm.
45. H. Mehrer, *Diffusion in Solids: Fundamentals, Methods, Materials, Diffusion Controlled Processes*, Vol. 155 (Berlin: Springer, 2007), p. 651.
46. J.M. Poate, K.N. Tuaaa, and J.W. Meyer, eds., *Thin Films-Interdiffusion and Reaction* (New York: Wiley, 1978), p. 578.
47. M. Garbrecht, B. Saha, J.L. Schroeder, L. Hultman, and T.D. Sands, *Sci. Rep.* 7, 46092-1 (2017). https://doi.org/10.1038/srep46092.
48. A. Makovec, G. Erdélyi, and D.L. Beke, *Thin Solid Films* 520, 2362 (2012). https://doi.org/10.1016/j.tsf.2011.11.013.
49. G. Molnár, G. Erdélyi, G.A. Langer, D.L. Beke, A. Csik, G.L. Katona, L. Daróczi, M. Kis-Varga, and A. Dudás, *Vacuum* 98, 70 (2013). https://doi.org/10.1016/j.vacuum.2013.04.015.
50. D.L. Beke, Yu Kaganovskii, and G.L. Katona, *Prog. Mater Sci.* 98, 625 (2018). https://doi.org/10.1016/j.pmatsci.2018.07.001.
51. A.I. Gusev and A. Rempel, *Nanocrystalline Materials* (Cambridge: Cambridge International Science, 2004), p. 351. ISBN: 978-1898326267.
52. J.H. Fendle, eds., *Nanoparticles and Nanostructured Films: Preparation, Characterization, and Applications* (Weinheim: Wiley, 2008), p. 488. ISBN 978-3-527-61206-2.